Lab on a Chip

PAPER

View Article Online
View Journal | View Issue

Cite this: *Lab Chip*, 2019, **19**, 1406

Label-free separation of leukocyte subpopulations using high throughput multiplex acoustophoresis†

Anke Urbansky, [a] Franziska Olm, [b] Stefan Scheding,[bc] Thomas Laurell*[a] and Andreas Lenshof *[a]

Received 20th February 2019,
Accepted 6th March 2019

DOI: 10.1039/c9lc00181f

rsc.li/loc

Multiplex separation of mixed cell samples is required in a variety of clinical and research applications. Herein, we present an acoustic microchip with multiple outlets and integrated pre-alignment channel to enable high performance and label-free separation of three different cell or particle fractions simultaneously at high sample throughput. By implementing a new cooling system for rigorous temperature control and minimal acoustic energy losses, we were able to operate the system isothermally and sort suspensions of 3, 5 and 7 μm beads with high efficiencies (>95.4%) and purities (>96.3%) at flow rates up to 500 μL min^{-1} corresponding to a throughput of ~2.5×10^6 beads per min. Also, human viable white blood cells were successfully fractionated into lymphocytes, monocytes and granulocytes with high purities of 96.5 ± 1.6%, 71.8 ± 10.1% and 98.8 ± 0.5%, respectively, as well as high efficiencies (96.8 ± 3.3%, 66.7 ± 3.2% and 99.0 ± 0.7%) at flow rates up to 100 μL min^{-1} (~100 000 cells per min). By increasing the flow rate up to 300 μL min^{-1} (~300 000 cells per min) both lymphocytes and granulocytes were still recovered with high purities (92.8 ± 1.9%, 98.2 ± 1 .0%), whereas the monocyte purity decreased to 20.9 ± 10.3%. The proposed isothermal multiplex acoustophoresis platform offers efficient fractionation of complex samples in a label-free and continuous manner at thus far unreached high sample throughput rates.

Introduction

White blood cells (WBC), leukocytes, play an important role in the human immune system and can be divided into three main subpopulations: lymphocytes, monocytes, and granulocytes. Immediate and individual access to these WBC subtypes holds significant value in research as well as clinical applications, such as lymphocyte purification for diagnostic purposes, or widely-applied standard lymphocyte function tests and gene expression analysis. In clinical cell processing WBC subtypes are used for manufacturing chimeric antigen receptor T cells in immunotherapy,[1] for monocyte enrichment to generate dendritic cells used in immunotherapy,[2] and for separation of granulocytes for transfusion.[3,4] However, methods that offer rapid, simultaneous and label-free separation of the three blood cell subsets, in limited sample volumes, still pose an unmet need.

Common separation methods such as fluorescence activated cell sorting (FACS) and magnetic activated cell sorting (MACS) require labeling of the cells, they are time consuming, expensive and require trained personnel. Microfluidic systems offer an alternative to label-based and/or affinity-based separation methods and can be used for multiplex separation of cells based on their physical properties such as size, density, shape, deformability, compressibility, charge, polarizability and magnetic susceptibility. Multiplex separation of different particle types with high efficiency and purity has been shown for several microfluidic devices such as deterministic lateral displacement (DLD),[5–8] inertial microfluidics,[9,10] dielectrophoresis (DEP),[11–13] acoustophoresis[14–16] or combinations of different forces and flow designs.[17,18] However, working with complex cell suspensions is often more difficult due to larger variation and overlaps in the biophysical cell properties. Previous reports on multiplex separation of lymphocytes, monocytes, and granulocytes at throughputs that meet bioanalytical or clinical needs have shown only limited success. Ramachandraiah *et al.*[10] used selective RBC lysis combined with inertial microfluidics to separate the three WBC subpopulations with fair purities (86% granulocytes, 43% monocytes, 91% lymphocytes) but only modest separation efficiencies (27% granulocytes, 90% monocytes, 53% lymphocytes) indicating a loss of especially granulocytes and lymphocytes in their system. Grenvall *et al.*[15] has demonstrated separation of WBC using pre-aligned free flow acoustophoresis. While this system showed sufficient

[a] *Department of Biomedical Engineering, Lund University, Lund, Sweden. E-mail: thomas.laurell@bme.lth.se, andreas.lenshof@bme.lth.se*
[b] *Department of Laboratory Medicine, Lund Stem Cell Center & Molecular Hematology, Lund University, Lund, Sweden*
[c] *Department of Hematology, University Hospital Skåne, Lund, Sweden*
† Electronic supplementary information (ESI) available. See DOI: 10.1039/c9lc00181f

separation efficiencies for lymphocytes and granulocytes but low monocyte purity, the maximum throughput was only 8 μL min^{-1} sample flow at a cell concentration of 10^6 cells per mL, *i.e.* 8000 cells per min.

In acoustophoresis, commonly a half-standing wave field is generated across a microchannel with a pressure node in the center of the channel and a pressure anti-node along the channel walls. The standing wave-induced acoustic radiation force moves cells or particles based on their size, density and compressibility in relation to their surrounding medium.[19] Typically, larger and denser particles experience higher acoustic forces and move faster towards the pressure node as compared to smaller and less dense particles. Based on the differences in the acoustophoretic mobility the various particles will end up in different lateral positions (stream lines) at the end of the microchannel and can there be collected into different outlets.

At higher throughput, the retention time for each particle in the sound field is reduced and thus the acoustic force has shorter time to act on the particle. To compensate for this, an increased channel length or higher actuation voltage can be employed. However, at higher voltages power dissipation in the electro-mechanical conversion in the transducer may result in elevated temperatures that require temperature control of the system.

In this paper, we describe multiplex separation in a multi-outlet acoustofluidic microchannel integrated with an acoustic pre-alignment channel. To allow operation of the piezoceramic actuator at elevated voltages a new air-cooling unit has been realized which alleviates thermal limitations in the system and thus enables a significantly increased sample throughput at unperturbed precision. In this study, we demonstrate high throughput multiplex acoustophoresis for particle mixtures as well as viable WBC.

Materials and methods

Acoustophoretic setup

The microfluidic structure was fabricated using deep reactive ion etching (Micronit, Enschede, Netherlands) and comprised a sample inlet, a pre-focusing channel (22 mm × 300 μm × 150 μm), a v-shaped flow splitter preceding the center buffer inlet and a main separation zone (30 mm × 375 μm × 150 μm) leading towards three outlets at the end of the channel (Fig. 1). The chip was sealed by anodic bonding of a glass lid and silicon tubings were glued to each inlet and outlet at the bottom of the microchannel as docking ports for the fluidic tubings. A pressure driven unit (VEMA-LS-8N3-9-D1-M5-22D9, Festo AB, Sweden) with flow sensor (SLI-1000 and SLI-2000 liquid flow meters, Sensirion AG, Switzerland) based

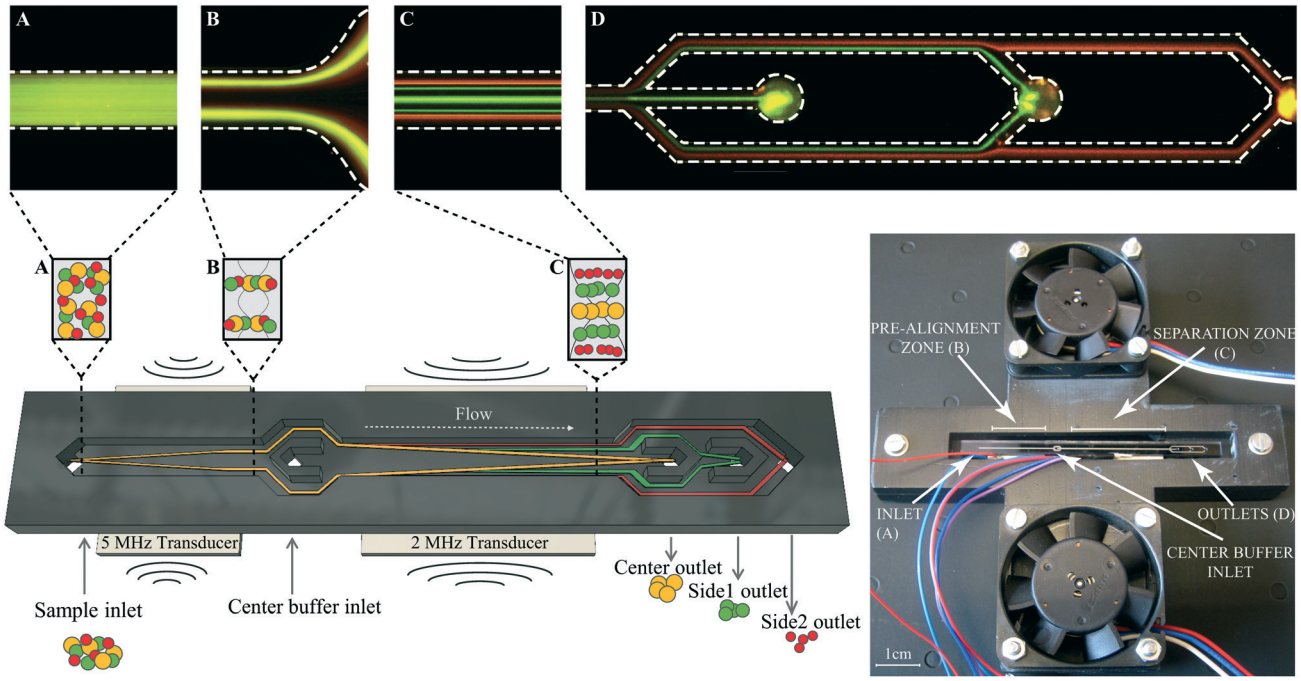

Fig. 1 Microfluidic chip and holder design. The schematic drawing shows the principle of multiplex acoustophoresis with acoustic pre-focusing as implemented in this study. A sample is injected into the microchannel (A) and the particle/cells are pre-aligned in width and height (B) before entering the main separation channel. Acoustic forces within the half-standing wave field in the separation channel will move the particles towards the pressure node in the center of the channel based on their acoustophysical properties (C and D). Larger and denser particles move faster in the sound field and can be collected into the center outlet (yellow) while medium sized particles move to side1 outlet (green) and the smallest particles are collected in side2 outlet (red). Fluorescence images (inserts in the top of the figure) were taken at different positions within the microchannel while acoustically separating 2 μm (red fluorescence), 4 μm (green fluorescence) and 6 μm (green fluorescence) beads, respectively, to support the schematic drawing. The picture on the lower right side shows the top view of the microfluidic chip holder with the positions of the inlets (A) and outlets (D) as well as the pre-alignment zone (B), the main separation zone (C), and the air-cooling fans.

feedback loop control (in-house build) was used to control the flow rates of the system. The flow rates at the different inlets and outlets for bead separation were set to 100 μL min^{-1} sample in, 300 μL min^{-1} center buffer in, 150 μL min^{-1} center out, 85 μL min^{-1} side1 out and 165 μL min^{-1} side2 out. Bead experiments at increased sample throughput were run by keeping the same split ratios at the inlets and outlets. Cell experiments were performed at 100 μL min^{-1} sample in, 300 μL min^{-1} center buffer in, 150 μL min^{-1} center out, 30 μL min^{-1} side1 out, and 220 μL min^{-1} side2 out. The acoustophoretic standing wave field was generated using piezoceramic transducers glued underneath the pre-focusing channel (resonant at 5 MHz) and main separation channel (resonant at 2 MHz). Both transducers were driven by a dual channel function generator (AFG3022B, Tektronix, Beaverton, OR, USA), connected to signal amplifiers (in-house build), and a two-channel digital oscilloscope (TDS 1002, Tektronix) was used to measure the voltage over each transducer. Temperature was monitored *via* PT1000 resistance temperature detectors attached to the side of the chip above the pre-alignment and main separation transducer. For visual inspection of the microchip and for taking fluorescence images a SZX10 stereo microscope equipped with a GFP filter, a XC10 camera (all Olympus, Tokyo, Japan), and a X-Cite 120Q excitation light source (Lumen Dynamics, Excelitas Technologies, Waltham, MA, USA) was used.

Holder design

The chip holder was designed in a 3D-CAD software (Autodesk Fusion 360) and 3D-printed (Ultimaker2, Ultimaker, Netherlands) in two pieces; the bottom piece contained air flow channels, the top piece had two open air conduits where two axial fans (Papst 412F2H, Elfa Distrelec, Sweden) were mounted, see supporting Fig. S1A.† The acoustofluidic chip was placed in the center slit of the chip holder. Besides four supportive regions where the tubings exit the chip, the chip is free hanging with open air vents above and below the chip. The fans push air through the manifold that exits through the top and bottom center slits where the chip is placed, see supporting Fig. S1B.†

Beads

Polystyrene beads in sizes 3, 5 and 7 μm (Sigma-Aldrich, St. Louis, MO, USA) were mixed equally in MilliQ + 0.01% Triton-X-100 (Sigma-Aldrich) and used as reference validation of the separation performance of the multiplex acoustophoresis chip.

For fluorescence images, Fig. 1, FITC-marked melamine resin micro particles in sizes 4 and 6 μm (Fluka, Sigma-Aldrich) and 2 μm Fluoro-Max red fluorescence polymer microspheres (Thermo Fisher Scientific, Waltham, MA, USA) were used.

Blood sample collection

Sample collection was approved by the Regional Ethical Review Board at Lund University, Sweden. Blood samples were obtained from healthy volunteers after informed consent at Lund University Hospital, Lund, Sweden and collected in vacutainer tubes (BD Bioscience, San Jose, CA, USA), containing ethylenediaminetetraacetic acid (EDTA) as anticoagulant.

White blood cell preparation and flow cytometric analysis

White blood cells (WBC) were obtained by selective lysis of red bloods cells using either BD Pharm Lyse lysing solution (BD Bioscience) for viable, non-fixed WBC samples, or BD FACS lysing solution (BD Bioscience) for fixed WBC preparation according to manufacture instructions. Cells were stained with monoclonal antibodies for 15 min at room temperature in the dark and adjusted to 1×10^6 cells per ml in 1× PBS + 2 mM EDTA + 0.01% BSA (Sigma-Aldrich). The following directly conjugated monoclonal antibodies were used: CD3-APC (clone HIT3a), CD14-PE (clone MφP9), CD19 FITC (clone HIB19), CD45-PerCP (clone 2D1), and CD66b FITC (clone G10F5), as well as matched isotype controls (all from BD Bioscience). Propidium iodide (Sigma-Aldrich) was used as a dead cell marker in viable WBC experiments. Immunofluorescent labeled samples were analyzed before and after acoustic separation on a FACSCanto II flow cytometer (BD Bioscience) and the acquired data were analyzed using FlowJo software (Tree Star Inc., Ashland, OR, USA).

Cell property measurements

Lymphocyte, monocyte and granulocyte populations were separated using acoustophoresis and purities were determined using a flow cytometer (all >90%). The size distribution of each cell fraction was measured with a Multisizer 3 Coulter Counter (Beckman Coulter, Brea, CA, USA), see Fig. S2.†

Statistics

If not otherwise stated, data are presented as mean ± standard deviation (SD) with $n = 3$ biological replicates and three technical repeats each.

Separation performance parameters

Separation performance parameters are reported as separation efficiency linked to the purity of that same collected fraction, where separation efficiency is calculated as the ratio of the number of desired particles per cells in a target outlet to the total number of desired particles per cells found in all outlets. Purity is defined as the ratio of the number of desired particles/cells to the total number of particles in a collected fraction. Furthermore, to also disclose system throughput in an unbiased manner we report the sample input volumetric flow rate and the particle/cell concentration of that same input sample. Mixing ratio of bead suspensions is given and for blood cell samples the initial sample as well as each collected fraction is presented with full FACS data.

Results and discussion

1. Thermal characterization of the cooling unit

Temperature stability is of importance in acoustofluidic systems as temperature drift alters the speed of sound of the

processed liquid, which in turn affects the resonance of the acoustophoresis channel. That is, a change in temperature causes a resonance frequency drift which results in a decrease in acoustic energy in the channel and thus the acoustic force acting on the particles is altered. Augustsson *et al.*[20] observed the shift in the acoustic resonance peak to be ~1 kHz °C^{-1} and a complete change of the resonance mode at temperature changes of 5 °C.

An increase of system temperature may originate from several sources. However, most prominently from losses in the piezo-mechanical coupling, where an increased voltage level will cause mechanical losses in the piezo ceramic that give rise to elevated temperatures. To counteract this temperature drift and maintain a constant level is thus very important.[20] Previously reported ways of cooling the chip have included the use of an aluminum chip holder with a Peltier element in proximity to the chip and a temperature sensor mounted on the piezo ceramic element linked to a feedback-loop control.[21] Although this design provided a successful temperature control, the clamping of the chip to the holder dissipated acoustic energy from the chip and thus the full potential of the acoustic energy input was not utilized. Work by Fong *et al.*[22] also reported the use of a fan located 2 cm from the chip to cool their acoustophoresis chips when driving the piezo actuator in the range of 1.4–1.8 MHz at voltages up to 23 V_{pp} and a 2 °C temperature variation. Without the fan, temperatures up to 70 °C were reported.

To alleviate the shortcomings of 1) a gradually rising temperature of the acoustophoresis system (red trace, Fig. 2A) causing a drift in optimal resonance frequency and 2) the acoustic power dissipation through the peltier/aluminium manifold, we have designed a 3D-printed air cooling manifold where the chip is free-hanging, suspended only in the connecting tubings. Furthermore, since the chip is positioned in an ambient air-flow path, the chip temperature stabilises a few degrees above ambient conditions (purple trace) within ~30 seconds. Two features transport heat from the acoustofluidic chip in operation: a) the liquid flowing through the chip and b) the fan driven convective transport of room tempered air across the chip (Fig. S1B†). Fig. 2A shows the impact of these different cooling aspects. At stop flow and no air cooling (red line), the temperature has not reached steady state even after four minutes of operation. With fluid flow active and no air cooling (blue line) the temperature levels out after 60 seconds at a five degree elevated temperature. Once the air fans are in operation the cooling effect is rapid, reaching steady state after 30 seconds at about two degree elevated chip temperature, and most notable the fluid flow at 800 μl min^{-1} through the chip does not significantly impact the system temperature, c.f. purple line *vs.* green line.

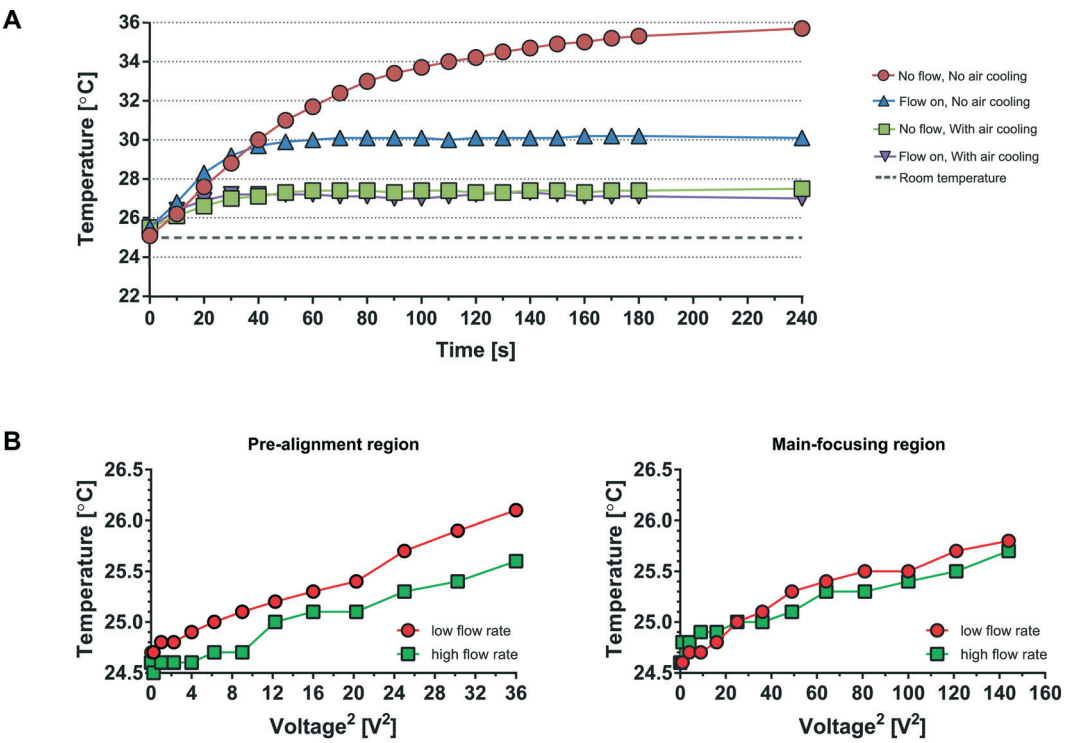

Fig. 2 Thermal characterization – (A) effects of cooling aspects at 800 μL min^{-1} total flow rate. Red: Without any cooling and no flow; blue: with flow and no air cooling; green: with air cooling and no flow; purple: both air cooling and flow. The pre-alignment transducer was driven at 4.3 V_{pp} and the main separation transducer at 4.6 V_{pp}. (B) The effect of an increase of amplitude on the temperature at the pre-focusing transducer (left) and main-focusing transducer (right) was investigated at total flow rates of 400 μL min^{-1} (low flow rate, red) and 2 mL min^{-1} (high flow rate, green) with air cooling turned on. The amplitude range was chosen based on the lowest and highest values used within the bead per cell experiments and temperature was measured 30 s after starting the system (n = 1).

Furthermore, experiments were conducted to analyze the effect on the temperature by applying different voltages at the pre-alignment transducer and main-separation transducer (Fig. 2B). The temperature is plotted against the voltage squared (V^2) as V^2 is proportional to the acoustic energy in the channel. The temperature increases less than 1.5 °C between 0 voltage applied and 6 V_{pp} (Fig. 2B, left) for the pre-alignment transducer and 12 V_{pp} (Fig. 2B, right) for the main-separation transducer, whereas when operating the system without the air cooling active the temperature rises ≈5 °C already at an operating voltage of 4.6 V_{pp} (Fig. 2A blue line). Going from 4.6 V_{pp} to 12 V_{pp} corresponds to a 7× increase in delivered acoustic energy. It should be noted that the higher temperature increase of ≈2 °C in Fig. 2A (purple line) is due to the additional heating of the microscope light source which was not activated in the experiments for Fig. 2B where a maximum of 1.5 °C temperature increase was seen. The free-hanging chip solution combined with the increased length of pre-alignment channel, allowed to operate the device at increased acoustic energy, resulting in a significantly increased sample throughput.

2. Effect of pre-alignment voltage

The simultaneous acoustophoretic fractionation of three different targets has been reported previously by Petersson *et al.*[14] Separation efficiencies of 76–96% were reported with samples containing 3, 7, and 10 μm polystyrene (PS) beads. The modest performance can be explained by the lack of a pre-alignment step which aligns all particles into the same flow vector and minimizes the influence of particles moving at different velocities in the Poiseuille flow. This ensures that the particles have the same retention time in the separation channel. The acoustophoretic pre-alignment, introduced by Augustsson *et al.*,[21] was later utilized by Grenvall *et al.*[15] in order to achieve separation of particles and cells based purely on acoustophysical properties, thereby minimizing influence of Poiseuille flow based dispersion. This resulted in significantly improved separation performance, 88–98%, for 3, 7, and 10 μm beads which also enabled WBC fractionation at recoveries of 86.5%, 83.1% and 68.4% for lymphocytes, monocytes and granulocytes, respectively.[15] This acoustic device was short with a pre-alignment length of only 10 mm and separation length of 22 mm. This translated to short retention times in the sound field, which required the use of very low flow rates (8 μL min^{-1}) to achieve a reasonable separation performance.

The design reported herein includes a pre-alignment channel of 22 mm length, a factor of 2.2 longer as compared to the original report on pre-alignment by Augustsson *et al.*[21] and later by Grenvall *et al.*[15] The longer pre-alignment channel enables a proportionally higher flow rate at unchanged pre-alignment performance. To show the influence and importance of the pre-alignment for multiplex acoustophoresis, an experiment was conducted in which the pre-alignment voltage initially was set to zero (pre-alignment off) and then gradually increased up to 18 Volts squared, see Fig. 3. At 0 Volts, *i.e.* no pre-alignment, a large fraction of 7 μm particles (yellow) ended up in side outlet 1 instead of the center outlet and 5 μm particles (green) were collected in side outlet 2 instead of side outlet 1. As the pre-alignment voltage increases and all particles end up in the same flow vector before the separation channel, the separation of the three particle sizes was greatly improved, now only depending on the acoustophysical properties of the particles.

3. Bead separation efficiency *versus* flow rate

Previous publications on acoustic multiplex particle separation reported maximum sample flow rates of 10 μL min^{-1} [15] and 40 μL min^{-1}.[14] To test the performance of the multiplex acoustic chip reported here, an equal mixture of 3, 5 and 7 μm polystyrene beads at a total bead concentration of 10^6 beads

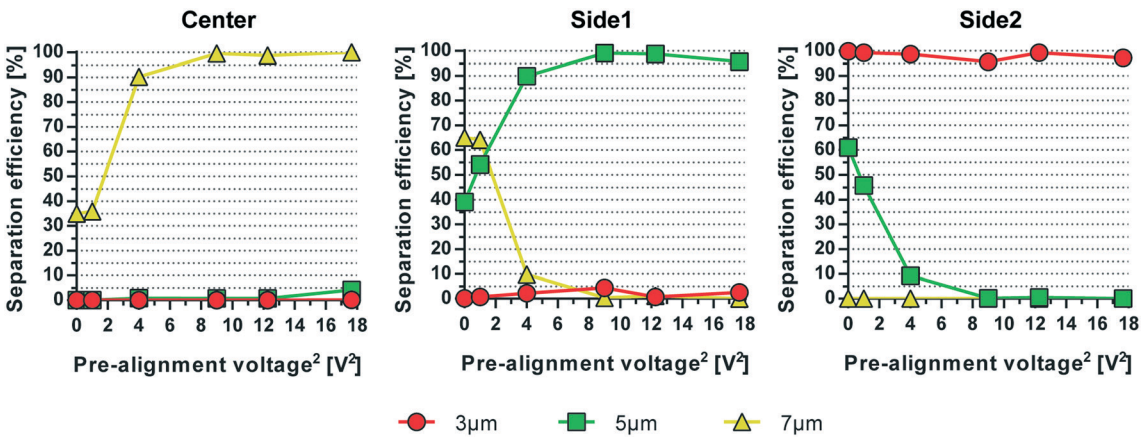

Fig. 3 Separation efficiency *vs.* pre-alignment voltage squared. At zero voltage, *i.e.* pre-alignment turned off, it is clearly visible that the separation efficiency is sub optimal with particle sizes ending up in several outlets. As the pre-alignment voltage is increased, all particles are effectively focused into the same flow vector with the same retention time in the main separation channel and thus the separation efficiency is purely determined by the acoustophysical properties of the particles. Note that the separation voltage controlling the one-dimensional standing wave was maintained constant at 4.5 V_{pp} and only the pre-alignment voltage was varied.

per mL was run through the chip at increasing sample flow rates. The split ratio of the inlets and outlets were fixed while the acoustic energy was increased such that the 7 μm beads exited through the center outlet, while the 5 μm beads were directed towards the side1 outlet and the 3 μm beads stayed along the channel wall and exited through the side2 outlet (Fig. 1). For sample flow rates up to 500 μL min^{-1} the mean separation efficiency, *e.g.* the number of desired beads in the target outlet compared to all three outlets, was >99.2% for 3 μm, >97.5% for 5 μm, and >99.9% for 7 μm, corresponding to mean purities of >98.7%, >99.3%, and >98.2% for 3, 5 and 7 μm, respectively (Fig. 4). At 600 μL min^{-1} a drop of system performance of up to 15% was observed mainly due to a contamination of 5 μm beads into the side2 outlet resulting in mean separation efficiencies (±SD) of 96.7 ± 2.6%, 82.4 ± 2.8% and 98.2 ± 0.1% and purities (±SD) of 83.5 ± 2.2%, 94.9 ± 2.4% and 98.5 ± 0.7% for 3, 5 and 7 μm, respectively. A possible explanation for the decrease in separation performance at higher flow rates is the increased flow instability due to the measuring range and accuracy of the flow sensors (SLI-1000: calibrated for ~80–1000 μl min^{-1} with 6% error, and SLI-2000: calibrated for ~200–5000 μl min^{-1} with 6.5% error) used to monitor the flow rate as well as the response time of the in-house built feed-back loop. Furthermore, at higher flow rates the beads may not have sufficient time in the pre-focusing channel to be pre-aligned in width and height before entering the main separation channel.

Recently, Wu *et al.*[23] combined acoustics and hydrodynamics to pre-align particles prior to multiplex particle separation using surface acoustic waves. Separation data on 10, 12 and 15 μm polystyrene beads showed purities around 90% for the different bead sizes in their target outlets. However, no data on bead concentration, flow rate, sample throughput and separation efficiency/recovery are given for the multiplex separation, which prevents a comparison of system throughput and performance to the system reported herein.

The acoustic radiation force acting on a particle scales with the particle radius to the third power (eqn (S1)†). Considering that previous multiplex acoustophoresis experiments were performed with bead sizes of 3, 7 and 10 μm, the separation shown in this paper with 3, 5 and 7 μm beads is more challenging due to the lower difference in acoustic mobility between the different bead sizes (eqn (S2)†). More precisely, in previous publications[14,15] the acoustic mobility of 3 and 7 μm polystyrene beads differed by a factor of ~5.44 and for 7 and 10 μm beads of ~2.04, while in this work the difference in mobility for 3 and 5 μm beads is only ~2.78, and for 5 and 7 μm beads ~1.96. Furthermore, compared to previous publications[14,15] an up to 60-fold increase in sample flow rate was achieved with comparable or even better separation performance.

4. Bead concentration influences separation efficiency

The initial sample concentration plays a crucial role for the separation outcome. Augustsson *et al.*[24] analyzed the washing efficiency, *i.e.* the transition of beads/cells from one laminated stream to another, for different particle concentrations and showed a constant drop of efficiencies at volume fractions >0.2%. This is in agreement with theoretical calculations from Ley and Bruus[25] which identified the threshold for the wash efficiency in acoustophoretic systems to be at around 1% particle volume fraction. At high particle concentrations the particle suspension starts to move as a whole due to hydrodynamic interactions between the particles. The migration velocity of a given particle towards the pressure node is lowered at higher particle concentrations while particles with lower acoustophoretic mobility are hydrodynamically coupled to faster moving particles. The effect of hydrodynamic interactions becomes even more crucial when trying to separate two different particle per cell types from each other. Magnusson *et al.*[26] reported a drop in performance when separating circulating tumor cells from white blood

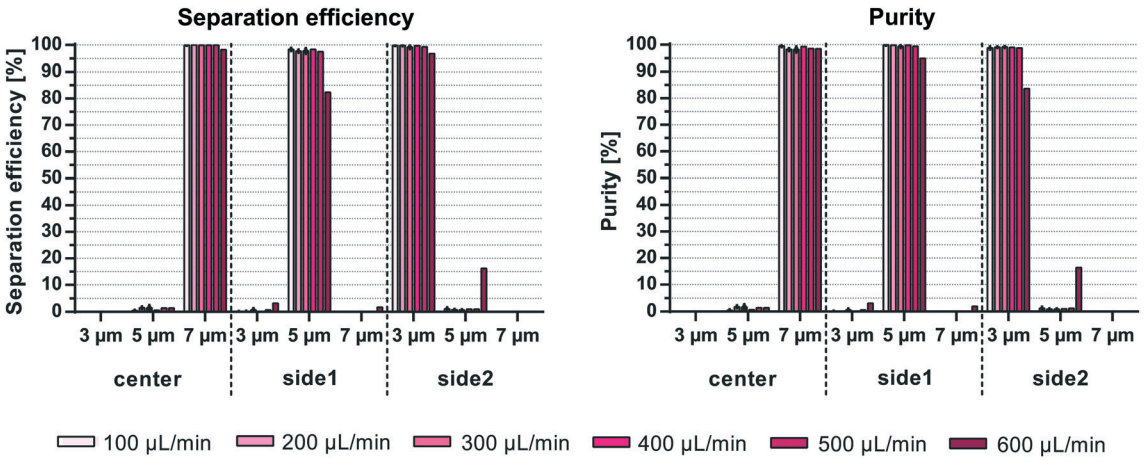

Fig. 4 Particle separation *vs.* flow rate. Acoustophoretic separation of an equal mixture of 3, 5 and 7 μm polystyrene beads at a total concentration of 10^6 beads per mL was performed at different sample flow rates varying the applied voltage squared from 25 to 130 at the main separation transducer. Shown are the separation efficiency, *i.e.* the number of particles collected in one outlet compared to all outlets, and the simultaneous purity of the targeted species at the three different outlets (n = 3, mean ± SD).

cells at an input concentration above 3.25×10^6 cells per mL, which corresponds to a volume fraction of ~0.2%.

Herein, system performance based on the initial sample concentration was investigated at 500 μL min^{-1} sample flow rate. Fig. 5 shows comparable separation efficiencies of >98.6% for 7 μm beads in the center outlet for sample concentrations up to 1.5×10^7 beads per mL (~0.13% volume fraction). However, the efficiency to separate 3 and 5 μm particles in side2 and side1 outlet, respectively, decreased with increasing sample concentrations from 99.3 ± 0.4% and 97.5 ± 0.5% at 1×10^6 beads per mL (~0.009% volume fraction) to 85.4 ± 0.8% and 89.1 ± 3% at 1.5×10^7 beads per mL (3 and 5 μm, respectively). Due to the carry-over of beads into non-target outlets the purity of 7 μm beads decreased from 98.5 ± 0.3% to 93.1 ± 2.2% with increasing sample concentrations, while the purity of 5 μm beads decreased from 99.3 ± 0.4% to 82.2 ± 6.9%. Only the purity of 3 μm beads remained between 99.8 ± 0.1% and 97.4 ± 1% in the side2 outlet. Similar to Magnusson *et al.*[26] the concentration limit for optimal separation is shown here to be below 0.2% volume fraction as compared to the 1% volume fraction in bead washing applications. Both Grenvall *et al.*[15] and Petersson *et al.*[14] used very high bead concentrations corresponding to 1.4 and 3.5–6% volume fraction, respectively, which could be one of the reasons for their lower separation outcome. Comparing the throughput of beads per min, we could reach up to 7.5×10^6 beads per min as compared to 1.5×10^6 beads per min[15] and 6×10^6–6.2×10^7 beads per min[14] with similar or better separation outcome despite working with a more challenging initial sample with small acoustic mobility differences between the beads (3, 5 and 7 μm beads used herein as compared to 3, 7 and 10 μm used previously).

5. Concurrent fractionation of white blood cells

Fractionation of white blood cells into lymphocytes, monocytes and granulocytes is of interest for various clinical and research applications. Acoustophoresis offers the possibility to simultaneously separate different particles and thus possibly also different blood cell types with high efficiencies and purities in limited sample volumes. Furthermore, acoustophoresis has been shown to be a gentle method which does not impact cell viability or functional capacity of the separated sample.[21,23,27–33]

There is a large size overlap between the different white blood cell populations with a median diameter (range) of 7.2 μm (5.5–10 μm) for lymphocytes, 9.5 μm (7.5–12 μm) for monocytes and 9.5 μm (8.5–11 μm) for granulocytes as determined by coulter counter measurements (Fig. S2†). The size differences are also reflected in corresponding scatter differences in fluorescent-activated flow cytometry analysis as shown in the histogram of the forward scatter signal (FSC) in Fig. 6A. The magnitude of the acoustic force acting on a particle is mainly depended on the particle size, which in this case would make it challenging to acoustically sort the three WBC subpopulations. However, also density and compressibility influence the acoustophoretic mobility of a particle. Typically, the density varies between 1.055–1.070 g cm^{-3} for monocytes and lymphocytes and 1.075–1.085 g cm^{-3} for granulocytes.[34] Based on these differences in the acoustic properties granulocytes show a higher acoustophoretic mobility in the acoustic standing wave field as compared to lymphocytes and move therefore faster towards the pressure node in the center of the microchannel where they can be collected in the center outlet. Lymphocytes on the other hand are less affected and stay close to the channel wall being directed to the side2 outlet. Monocytes show a more disperse acoustophoretic mobility and are mainly directed towards the side1 outlet.

Fractionation of viable WBC into lymphocytes, monocytes and granulocytes was shown successfully for different flow rates (Fig. 6B) without impairing the cell viability (98.4 ± 1.9% before and 98.2 ± 2.1% after separation). At 100 μL min^{-1} sample flow and a throughput of 100 000 cells per min 99 ± 0.7% of the granulocytes were translated to the center

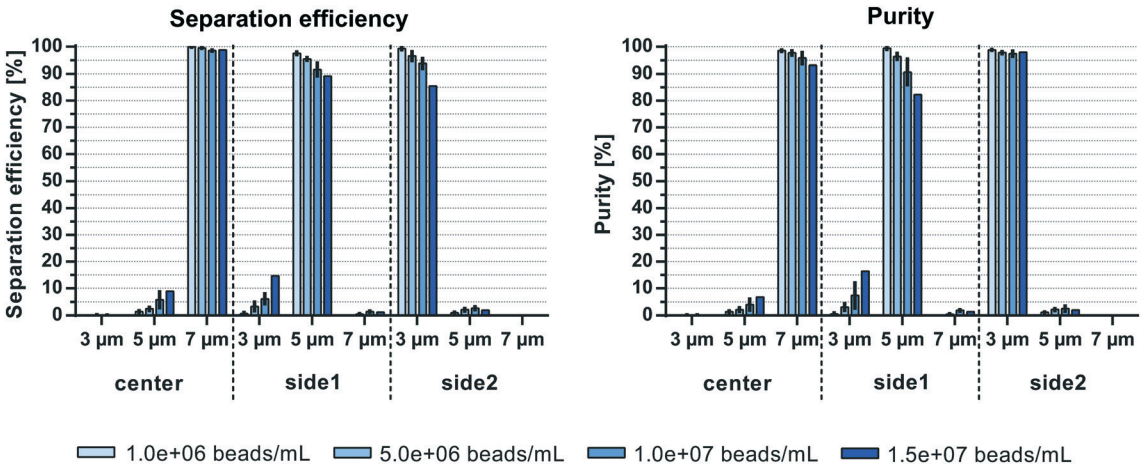

Fig. 5 Particle separation *vs.* sample bead concentration. Acoustophoretic separation of an equal mixture of 3, 5 and 7 μm polystyrene beads was performed at 500 μL min^{-1} sample flow while altering the initial sample concentrations. Shown are the separation efficiency and purity of the different beads in the three outlets (n = 3, mean ± SD).

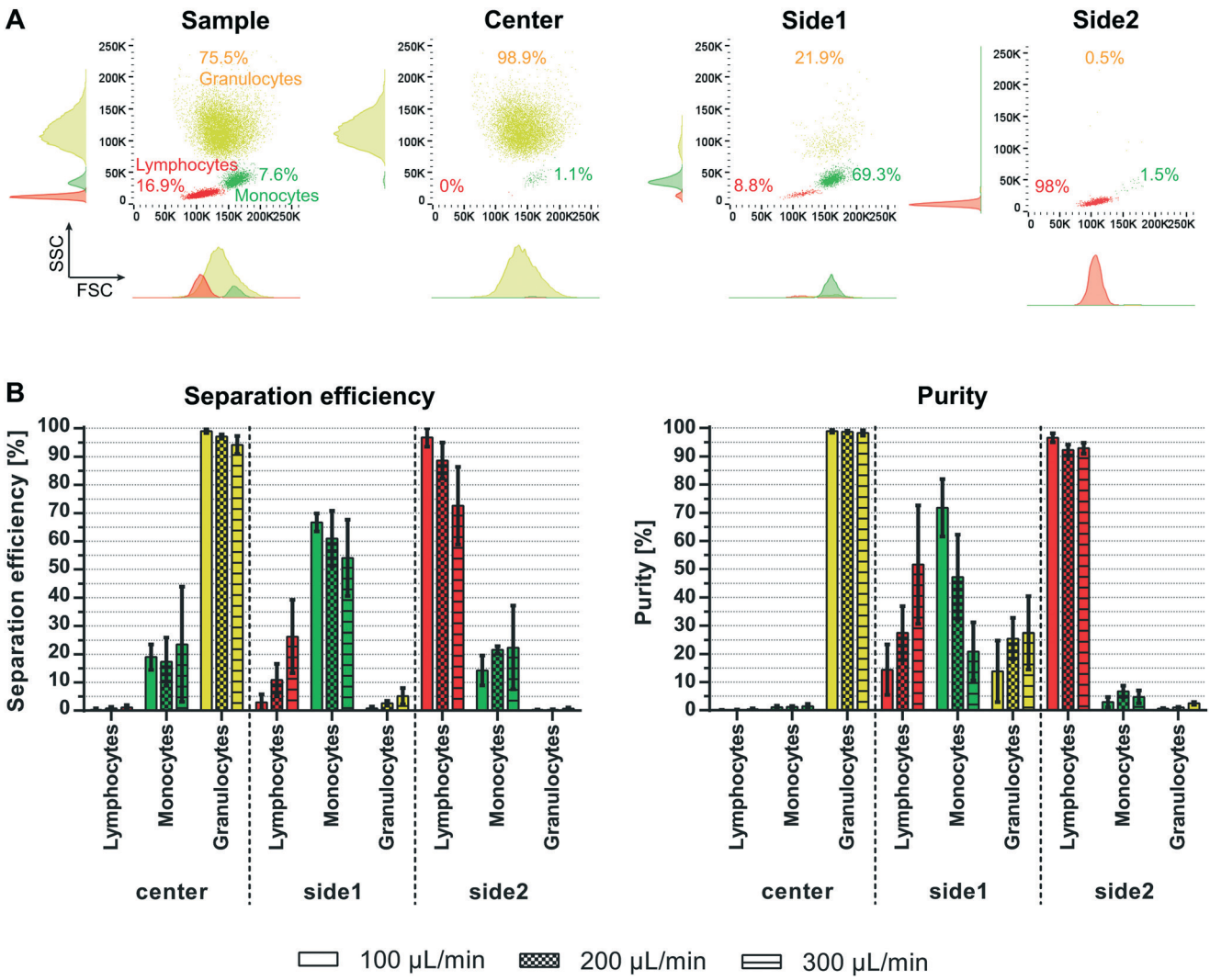

Fig. 6 Fractionation of viable white blood cell subpopulations. Simultaneous acoustophoretic separation of lymphocytes, monocytes and granulocytes from lysed whole blood at a starting concentration of 1×10^6 WBC per mL. (A) FACS plot analysis showing the forward scatter and side scatter plots of the input sample and the three different outlets for a typical run at 100 µL min^{-1} sample flow. (B) Shown are the separation efficiency and purity for varying sample flow rates (n = 3, mean ± SD).

outlet, 66.78 ± 3.2% of monocytes were directed towards the side1 outlet and 96.8 ± 3.3% of lymphocytes towards the side2 outlet. This corresponded to purities of 98.8 ± 0.5%, 71.8 ± 10.1% and 96.6 ± 1.6% for granulocytes, monocytes and lymphocytes, respectively. Increasing the sample flow rate, however, decreased the separation outcome. Especially lymphocytes tended to contaminate the side1 outlet resulting in a significantly lower purity of monocytes of 20.9 ± 10.3% and the larger drop in separation efficiency of lymphocytes to 72.6 ± 13.8% at 300 µL min^{-1} sample flow, maybe due to insufficient time for complete alignment in the pre-focusing channel before entering the main-separation channel. Ramachandraiah *et al.*[10] obtained similar purities of 91% for lymphocytes, 43% of monocytes and 86% of granulocytes using selective red blood cell lysis and inertial microfluidics. However, the reported separation efficiencies in their spiral microchannel indicated a considerable loss of granulocytes and lymphocytes in their system. We do see a shift in the WBC subpopulation ratio before and after the acoustic separation (Fig. S3†). However, this discrepancy is mainly seen at the lower sample flow rate of 100 µL min^{-1} (200 µL sample). Due to the considerably lower flow rate in the side1 outlet, *i.e.* the monocyte outlet, which is 30 µL min^{-1} out of 400 µL min^{-1} total flow and the dead volume in the sample tubing, not all monocytes are recovered into the side1 outlet tube. This effect will be evened out by running larger sample volumes, as seen for sample flow rates of 200 µL min^{-1} (400 µL sample) and 300 µL min^{-1} (600 µL sample), or by flushing the remaining cells in the tubing's after the acoustic run. Compared to previous acoustophoretic multiplex separation of leukocyte subpopulations, a higher separation efficiency for lymphocytes and granulocytes was achieved at high flow rates up to 200 µL min^{-1} (200 000 cells per min) with comparable purities for the two subpopulations as well as higher

purity for monocytes. Even at 300 μL min^{-1} (300 000 cells per min) comparable outcomes were achieved with separation efficiencies of 94.1 ± 3.2%, 54.1 ± 13.5% and 72.6 ± 13.8%, and purities of 98.2 ± 1%, 20.9 ± 10% and 92.8 ± 1.9% for granulocytes, monocytes and lymphocytes, respectively. This corresponds to flow rates that were 37.5 fold faster and a 37.5 fold faster cell throughput per minute than previously reported.[15]

However, it should be noted that Grenvall *et al.* used fixed cells in the experiments (8 μL min^{-1}, 8000 cells per min). This is important, as we can see a shift in the forward scatter and side scatter signal in the flow cytometer indicating a different size distribution as well as granularity distribution between the different subpopulations when comparing fixed and viable WBC (Fig. S4†). Density and speed of sound measurements by Cushing *et al.*[35] furthermore revealed an increase in the compressibility as well as a decrease in the density and the acoustophoretic contrast factor for fixed cells as compared to viable cells. Taken the reduced size distribution and acoustophoretic contrast factor of fixed WBC into account an overall lower acoustophoretic mobility of fixed WBC in the acoustic standing wave field is expected. These results are in agreement with Augustsson *et al.*[21] who reported a difference in separation performance between fixed and unfixed WBC. Lower acoustic energy was needed to move viable cells, which displayed a higher acoustophoretic contrast factor, however a better separation outcome was obtained using fixed cells due to changes in the acoustic properties of the cancer cells after fixation. As a result of the apparently bigger size overlap of fixed white blood cell subpopulations (Fig. S4,† Fig. 7A) and the decrease in the acoustophoretic contrast factor we expected a less promising separation performance in our multi-outlet chip using fixed cells. Separation data confirmed the assumption that we cannot discriminate equally well between the three subpopulations using fixed WBC (Fig. 7B). With a sample throughput of 100 μL min^{-1} (100 000 cells per min) we achieved a separation efficiency of only 76.1 ± 13.3% for granulocytes, 56.4 ± 13.8% for monocytes and 85 ± 3.5% for lymphocytes with purities of 98 ± 0.7%, 12.6 ± 5.3% and 85.6 ± 14.8% for granulocytes, monocytes and lymphocytes, respectively. Especially the monocytes are more disseminated between all three different outlets. The magnitude of the acoustic field needed to be increased in order to optimally pre-focus the cells which is in agreement with the observation of Augustsson *et al.*[21] and the measurements of Cushing *et al.*[35] Possibly, the magnitude of the acoustic force in the pre-alignment channel of the multi-outlet chip was not sufficiently strong to completely focus the cells before entering the main separation channel, which is indicated in the

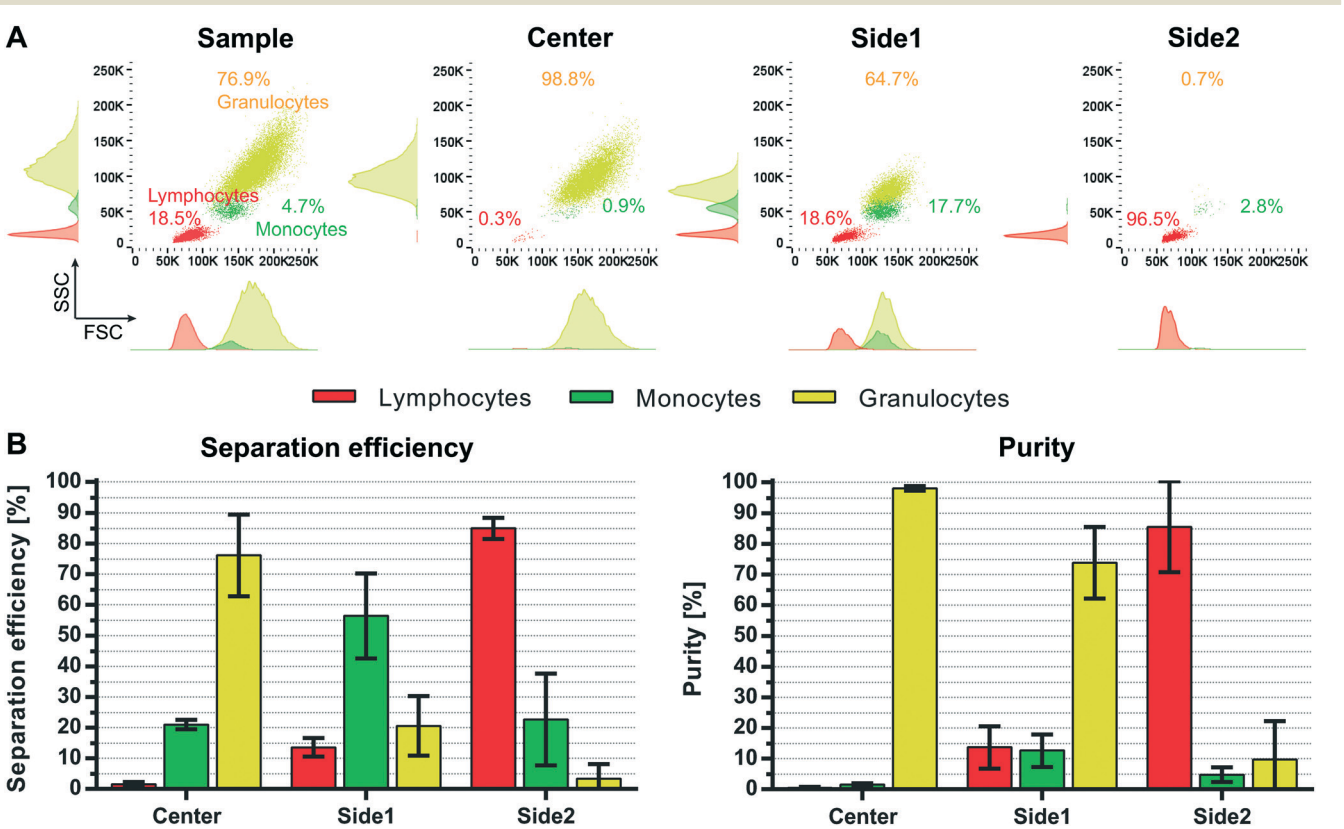

Fig. 7 Fractionation of fixed white blood cells. Acoustophoretic separation of lymphocytes, monocytes and granulocytes from lysed and fixed whole blood at a starting concentration of 1 × 10^6 WBC per mL. (A) FACS plot analysis showing the forward scatter and side scatter plots of the input sample and the three different outlets. (B) Shown are the separation efficiency and purity at 100 μL min^{-1} sample throughput (n = 3, mean ± SD).

increase of lymphocytes in the side1 outlet at elevated flow rates. Optimizing the running parameters such as flow rate, length of the pre-focusing channel and magnitude of the acoustic field may further increase the separation performance using fixed WBC.

Conclusion

We have demonstrated an acoustofluidic device with unsurpassed throughput for concurrent fractionation of WBC subpopulations. Sample flow rates were more than 10 times higher than in previously reported acoustofluidic devices for bead separation and more than 35 times higher for WBC fractionation (>35× higher cell throughput) at significantly better separation efficiency and purity. The novel design of the chip holder provided effective air cooling of the chip with minimal clamping of the acoustic device, which enabled more efficient utilization of the net input acoustic energy.

Author contributions

All authors conceived and discussed the method and experiments. A. U., F. O. and A. L. designed and performed the experiments and analyzed data. A. U. and A. L. wrote the manuscript and all authors edited the manuscript.

Conflicts of interest

There are no conflicts to declare.

Acknowledgements

This work was supported by the People Programme (Marie Curie Actions) of the European Union's Seventh Framework Programme FP7/2007-2013/under REA grant agreement no. 607350; the Knut Alice Wallenberg Foundation (Grant No. KAW 2012.0023); the Swedish Research Council (Grant No. 621-2014-6273); VINNOVA – CellCARE, (Grant No. 2009-00236); the University Hospital of Lund Funds; the ALF grant from the Medical Faculty at Lund University and the Carl Trygger Foundation (13:254). In addition, Scheding is a fellow of the Swedish Cancer Foundation (Cancerfonden).

References

1 B. L. Levine, J. Miskin, K. Wonnacott and C. Keir, *Mol. Ther.–Methods Clin. Dev.*, 2017, **4**, 92–101.
2 T. Felzmann, V. Witt, D. Wimmer, G. Ressmann, D. Wagner, P. Paul, K. Hiittner and G. Fritsch, *Cytotherapy*, 2003, **5**, 391–398.
3 A. A. Marfin and T. H. Price, *J. Intensive Care Med.*, 2015, **30**, 79–88.
4 D. Gurlek Gokcebay and S. Akpinar Tekgunduz, *Transfus. Apher. Sci.*, 2018, **57**, 16–19.
5 L. R. Huang, E. C. Cox, R. H. Austin and J. C. Sturm, *Science*, 2004, **304**, 987–990.
6 D. W. Inglis, J. A. Davis, T. J. Zieziulewicz, D. A. Lawrence, R. H. Austin and J. C. Sturm, *J. Immunol. Methods*, 2008, **329**, 151–156.
7 S. H. Holm, J. P. Beech, M. P. Barrett and J. O. Tegenfeldt, *Lab Chip*, 2011, **11**, 1326–1332.
8 D. Holmes, G. Whyte, J. Bailey, N. Vergara-Irigaray, A. Ekpenyong, J. Guck and T. Duke, *Interface Focus*, 2014, **4**, 20140011.
9 S. S. Kuntaegowdanahalli, A. A. S. Bhagat, G. Kumar and I. Papautsky, *Lab Chip*, 2009, **9**, 2973–2980.
10 H. Ramachandraiah, H. A. Svahn and A. Russom, *RSC Adv.*, 2017, **7**, 29505–29514.
11 K.-H. Han, S.-I. Han and A. B. Frazier, *Lab Chip*, 2009, **9**, 2958.
12 U. Kim, J. Qian, S. A. Kenrick, P. S. Daugherty and H. T. Soh, *Anal. Chem.*, 2008, **80**, 8656–8661.
13 N. Lewpiriyawong and C. Yang, *Electrophoresis*, 2014, **35**, 714–720.
14 F. Petersson, L. Aberg, A.-M. Swärd-Nilsson and T. Laurell, *Anal. Chem.*, 2007, **79**, 5117–5123.
15 C. Grenvall, C. Magnusson, H. Lilja and T. Laurell, *Anal. Chem.*, 2015, **87**, 5596–5604.
16 M. Wu, Y. Ouyang, Z. Wang, R. Zhang, P.-H. Huang, C. Chen, H. Li, P. Li, D. Quinn, M. Dao, S. Suresh, Y. Sadovsky and T. J. Huang, *Proc. Natl. Acad. Sci. U. S. A.*, 2017, **114**, 10584–10589.
17 J. D. Adams, P. Thévoz, H. Bruus and H. T. Soh, *Appl. Phys. Lett.*, 2009, **95**, 254103.
18 E. Ozkumur, A. M. Shah, J. C. Ciciliano, B. L. Emmink, D. T. Miyamoto, E. Brachtel, M. Yu, P. Chen, B. Morgan, J. Trautwein, A. Kimura, S. Sengupta, S. L. Stott, N. M. Karabacak, T. A. Barber, J. R. Walsh, K. Smith, P. S. Spuhler, J. P. Sullivan, R. J. Lee, D. T. Ting, X. Luo, A. T. Shaw, A. Bardia, L. V. Sequist, D. N. Louis, S. Maheswaran, R. Kapur, D. A. Haber and M. Toner, *Sci. Transl. Med.*, 2013, **5**, 179ra47–179ra47.
19 T. Laurell, F. Petersson and A. Nilsson, *Chem. Soc. Rev.*, 2007, **36**, 492–506.
20 P. Augustsson, R. Barnkob, S. T. Wereley, H. Bruus and T. Laurell, *Lab Chip*, 2011, **11**, 4152–4164.
21 P. Augustsson, C. Magnusson, M. Nordin, H. Lilja and T. Laurell, *Anal. Chem.*, 2012, **84**, 7954–7962.
22 E. J. Fong, A. C. Johnston, T. Notton, S.-Y. Jung, K. A. Rose, L. S. Weinberger and M. Shusteff, *Analyst*, 2014, **139**, 1192–1200.
23 M. Wu, K. Chen, S. Yang, Z. Wang, P.-H. Huang, J. Mai, Z.-Y. Li and T. J. Huang, *Lab Chip*, 2018, **18**, 3003–3010.
24 P. Augustsson, J. Persson, S. Ekström, M. Ohlin and T. Laurell, *Lab Chip*, 2009, **9**, 810–818.
25 M. W. H. Ley and H. Bruus, *Lab Chip*, 2016, **16**, 1178–1188.
26 C. Magnusson, P. Augustsson, A. Lenshof, Y. Ceder, T. Laurell and H. Lilja, *Anal. Chem.*, 2017, **89**, 11954–11961.
27 J. Dykes, A. Lenshof, I.-B. Åstrand-Grundström, T. Laurell and S. Scheding, *PLoS One*, 2011, **6**, e23074.

28 M. A. Burguillos, C. Magnusson, M. Nordin, A. Lenshof, P. Augustsson, M. J. Hansson, E. Elmér, H. Lilja, P. Brundin, T. Laurell and T. Deierborg, *PLoS One*, 2013, **8**, e64233.
29 A. Lenshof, A. Jamal, J. Dykes, A. Urbansky, I. Åstrand-Grundström, T. Laurell and S. Scheding, *Cytometry, Part A*, 2014, **85**, 933–941.
30 O. Jakobsson, S. S. Oh, M. Antfolk, M. Eisenstein, T. Laurell and H. T. Soh, *Anal. Chem.*, 2015, **87**, 8497–8502.
31 A. Urbansky, A. Lenshof, J. Dykes, T. Laurell and S. Scheding, *Micromachines*, 2016, **7**, 101.
32 C. Lissandrello, R. Dubay, K. T. Kotz and J. Fiering, *SLAS Technol.*, 2018, **23**, 352–363.
33 M. Wiklund, *Lab Chip*, 2012, **12**, 2018–2028.
34 P. Sethu, A. Sin and M. Toner, *Lab Chip*, 2006, **6**, 83–89.
35 K. W. Cushing, F. Garofalo, C. Magnusson, L. Ekblad, H. Bruus and T. Laurell, *Anal. Chem.*, 2017, **89**, 8917–8923.